Available online at www.sciencedirect.com
SCIENCE DIRECT®
Journal of Power Sources 119–121 (2003) 221–225
JOURNAL OF POWER SOURCES
www.elsevier.com/locate/jpowsour

Preparation of orthorhombic $LiMnO_2$ material via the sol–gel process

Z.P. Guo*, K. Konstantinov, G.X. Wang, H.K. Liu, S.X. Dou

Institute for Superconducting & Electronic Materials, University of Wollongong, Wollongong, NSW 2500, Australia

Abstract

Orthorhombic $LiMnO_2$ was synthesized via the sol–gel process using citric acid as a chelating agent. The effect of varying the molar acid to metal ions ratio (R) on the structural and electrochemical properties of the synthesized compound was studied. Samples with high R ($R = 1, 2$) contain large amount of MnO impurity phase, which is electrochemically inactive and thus is detrimental to the electrochemical activity of the electrode. Therefore, the acid to metal ions ratio "R" should not be high. Samples with low R ($R = 0.5$) exhibited a high initial capacity, above 190 mAh/g when cycled at a current density of 0.4 mA/cm^2 at room temperature. The ac impedance results show that the initial capacity was improved (compared with ss-o-$LiMnO_2$) due to the smaller particle size and good homogeneity, which improves the Li^+ diffusion in the cathode.

Keywords: Sol–gel; Acid to metal ions ratio (R); Orthorhombic $LiMnO_2$

1. Introduction

Lithium manganese oxide compounds are major candidates for low cost and safe cathode materials in lithium rechargeable batteries. Batteries utilizing the $LiMn_2O_4$ spinel compound have already been commercialized. $LiMn_2O_4$ spinel has shown excellent cycle performance at room temperature in the 4 V region. However, it shows a significant capacity loss when cycled in the (3 + 4) V region as well as at high temperature [1,2]. A tetragonal to cubic structure change occurs when the average manganese valence reaches about 3.5. It is the critical concentration of Mn^{3+} that leads to the Jahn–Teller distortion responsible for the change [3]. $LiMnO_2$ (both orthorhombic and monoclinic) materials exhibit better cycle performances than $LiMn_2O_4$ spinel when used over a wide voltage region [4,5]. A preliminary electrochemical study of orthorhombic samples (o-$LiMnO_2$) revealed a link between electrochemical performance and the crystallization state of this compound when used as the positive electrode in lithium secondary batteries [6]. Previous work had revealed that the smaller the sample crystals/crystallites, the more Li can be removed from the $LiMnO_2$, so that better electrode performance could be expected for o-$LiMnO_2$ with small crystallite/crystals [7].

Sol–gel synthesis is one of the promising solution-based methods that has been widely used to synthesize materials with good battery activity. Many transition metal oxides like $LiCoO_2$ [8], $LiNiO_2$ [9], and $LiMn_2O_4$ spinel [10], synthesized using the sol–gel process, have improved electrochemical performance. This kind of synthesis allows a better control of the morphology and texture of solid particles. Recently, we reported that $LiCoO_2$ material prepared by the sol–gel method showed good cyclability [11]. The present paper describes the structural and electrochemical properties of o-$LiMnO_2$ synthesized using citric acid as a chelating agent. Although o-$LiMnO_2$ has been widely studied, the synthesis of o-$LiMnO_2$ using citric acid as a chelating agent has not been reported to the best of our knowledge. Varying the acid to metal ion ratio and its effects on the structural and electrochemical properties of o-$LiMnO_2$ are described in detail.

2. Experimental

The o-$LiMnO_2$ material was synthesized using $Mn(CH_3COO)_2 \cdot 4H_2O$ (Aldrich 99.5%), $Li(CH_3COO) \cdot 2H_2O$ (Aldrich 99.5%) and citric acid (Aldrich 99%) as starting materials. $Mn(CH_3COO)_2 \cdot 4H_2O$ and $Li(CH_3COO) \cdot 2H_2O$ were weighed according to a cationic ratio 1:1 and made into a saturated solution in ethyl alcohol. The extensively mixed alcoholic solutions of lithium and manganese acetate, and citric acid were added to alcohol under constant stirring. The acid to metal ions ratio R was set at 0.5, 1 and 2 for the various samples. The mixture was then heated under constant stirring at 80 °C for 2 h, which made the mixture denser and formed

* Corresponding author. Fax: +61-2-4221-5731.
E-mail address: zg04@uow.edu.au (Z.P. Guo).

0378-7753/03/$ – see front matter © 2003 Elsevier Science B.V. All rights reserved.
doi:10.1016/S0378-7753(03)00237-4

the "gel". The gel was heated at 110 °C under vacuum for 4 h. The dried gel was collected and subjected to further heat treatment at 800 °C for 12 h under a flow of argon.

Powder X-ray diffraction (1730 X-ray diffractometer) using Cu Kα radiation was employed to identify the crystalline phase of the synthesized materials. The particle morphologies of the resulting compound were observed using a scanning electron microscope (SEM).

The electrochemical characterizations were performed using Teflon cells. The cathode was prepared by mixing *o*-$LiMnO_2$ powder with 10 wt.% carbon black and 5 wt.% polyvinylidene fluoride (PVDF) solution. The *o*-$LiMnO_2$ and carbon black powders were first added to a solution of PVDF in *N*-methyl-2-pyrrolidinone (NMP) to make a slurry with appropriate viscosity. The mixture was then coated on to Al foil. After the electrode was dried at 140 °C for 2 h in vacuum, it was compressed at about 150 kg/cm^2. Teflon test cells were assembled in an argon filled glove box, where the counter electrode was Li metal and the electrolyte was 1 M $LiPF_6$ dissolved in a 50/50 vol.% mixture of ethylene carbonate (EC) and dimethyl carbonate (DMC). These cells were cycled between 2.0 and 4.4 V at room temperature to measure the electrochemical response. The ac impedance measurements were carried out utilizing an EG&G Model 6310 electrochemical impedance analyzer. Electrochemical impedance software (EG&G Model 398) was used to control a computer for conductivity and stability measurements. The ac impedance was measured potentiostatically over a frequency range of 100 kHz to 0.01 Hz at six points per decade of frequency with a 5 mV ac input signal applied between the working and reference electrodes.

3. Results and discussions

3.1. Crystal structure

The X-ray patterns recorded for the synthesized compounds with different *R* values compared to those of *o*-$LiMnO_2$ prepared by solid-state reaction are shown in Fig. 1. The main peaks for the orthorhombic phase are labeled with their *hkl* indices. Positions for peaks characteristic of monoclinic Li_2MnO_3 phase and MnO are indicated. Compared with the *o*-$LiMnO_2$ prepared by solid-state reaction with Li/Mn $= 1.05$ calcined at 1000 °C for 12 h (ss-*o*-$LiMnO_2$), no significant broadening of the XRD peaks in sg-*o*-$LiMnO_2$ (*o*-$LiMnO_2$ prepared by sol–gel method) was observed. A monoclinic Li_2MnO_3 phase was observed in XRD patterns for the solid-state reaction sample and the sol–gel sample with $R = 0.5$. With *R* increased to higher values, no Li_2MnO_3 impurity phase was observed in the XRD patterns, but a MnO phase emerged; MnO peaks merged with (1 1 0), (1 1 1) and (1 3 0) peaks from *o*-$LiMnO_2$, so that three strong peaks can be observed in the XRD patterns. Possible reasons for this could be that, with larger *R* values, the amount of the organic groups increased in the precursors. These organic groups could react during sintering with free oxygen (diluted in argon) and yield CO_2 [12], thus decreasing the oxygen content of the gas. Tang et al. reported that the transformation of *o*-$LiMnO_2$ into a mixture of $LiMn_2O_4$ and Li_2MnO_3 was accompanied by the absorption of oxygen gas during the calcination process ($3LiMnO_2 + (1/2)O_2 \rightarrow Li_2MnO_3 + LiMn_2O_4$) [13]. Therefore, a decrease of oxygen content in atmosphere will reduce the impurity phase Li_2MnO_3. On the other hand, with decreases in the partial pressure of oxygen, samples contain MnO impurity phase because of the stronger reducing conditions [14]. In practice, it is not easy to control the formation of a single-phase $LiMnO_2$ product under these conditions. This is consistent with the attempts of Barboux et al. to synthesize $Li_2Mn_2O_4$ from manganese acetate and lithium acetate by annealing the reagents at 400 °C at low oxygen pressures in argon [15]. The presence of large amounts of MnO could be detrimental to the electrochemical activity of the spinel electrode, because MnO is electrochemically inactive. Therefore, the ratio between acid and metal ions should not be too high (lower than 1). Other phenomena observed from the XRD patterns are that the intensity ratios of the (0 2 1)/(1 0 1) and

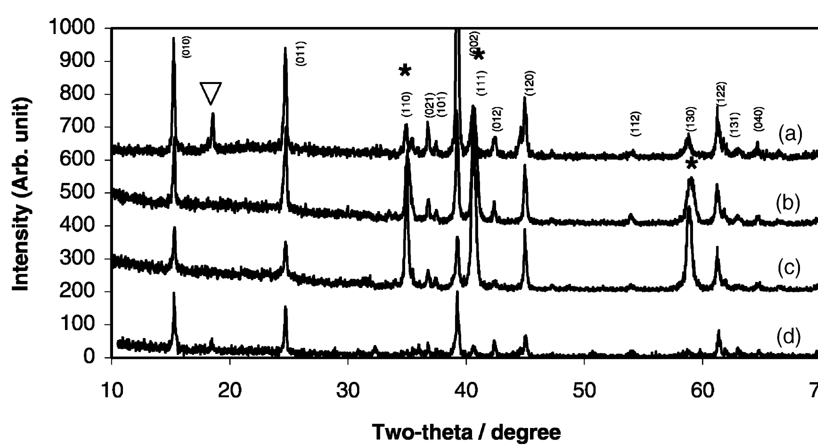

Fig. 1. XRD patterns of sg-*o*-$LiMnO_2$ and ss-*o*-$LiMnO_2$ materials (Li/Mn $= 1.05$ in precursor, and ss-*o*-$LiMnO_2$ material calcined at 1000 °C for 12 h). (▽) Monoclinic Li_2MnO_3, (∗) MnO. (a) ss-*o*-$LiMnO_2$; (b) sg-*o*-$LiMnO_2$, $R = 2$; (c) sg-*o*-$LiMnO_2$, $R = 1$; (d) sg-*o*-$LiMnO_2$, $R = 0.5$.

Table 1
Orthorhombic unit cell parameters (Å) for $LiMnO_2$ materials prepared by the sol–gel method with different *R* ratios (*R*: molar ratio of the acid to metal ions)

	a	*b*	*c*
$R = 2$	2.805 ± 0.001	5.752 ± 0.001	4.593 ± 0.001
$R = 1$	2.802 ± 0.001	5.754 ± 0.001	4.588 ± 0.002
$R = 0.5$	2.801 ± 0.001	5.750 ± 0.002	4.583 ± 0.002
Solid-state reaction sample	2.806 ± 0.001	5.755 ± 0.002	4.574 ± 0.001

(0 0 2)/(0 1 2) peaks from the different *o*-$LiMnO_2$ samples are different. Although the differences in the intensity ratios of peaks can still not be conclusively explained, we believe that different preparation methods caused different degrees of structural disorder. The *o*-$LiMnO_2$ phase has a distorted cubic close-packed oxygen array with alternating zigzag layers of Li and Mn cations. Unit cell parameters for the orthorhombic $LiMnO_2$ phases are reported in Table 1. It was found that different preparation methods affect the overall lattice constants of *o*-$LiMnO_2$. The change in acid to metal ion ratio (*R*) has a direct impact on pH, and solution-based synthesis methods are sensitive to pH, which determines the formation of the compound as well as its electrochemical performance. On the other hand, the self-igniting property of the organic groups involved in the precursors has a direct effect on the oxygen partial pressure during synthesis. The sudden variation in the oxygen partial pressure has an effect on the compound formation.

The scanning electron micrographs (SEM) of *o*-$LiMnO_2$ powders calcined at 800 °C for 12 h for different *R* are similar. (A typical SEM image is shown in Fig. 2b.) Compared with the particle sizes from the SEM image of ss-*o*-$LiMnO_2$ (2–15 μm) (Fig. 2a), the sol–gel method particle size is much smaller (below 200 nm). The micrograph shows homogeneous distribution of the particles.

(a)
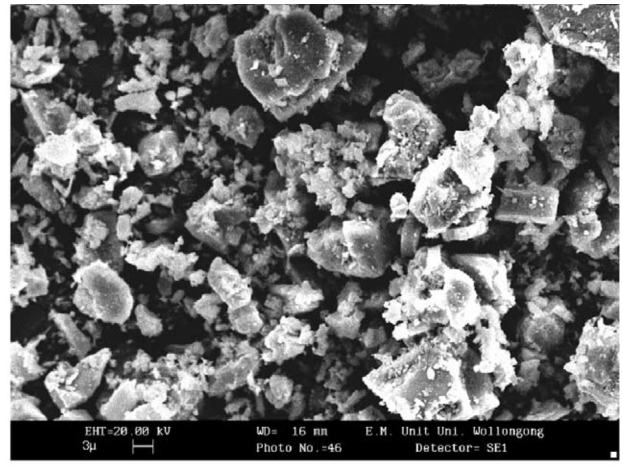

(b)
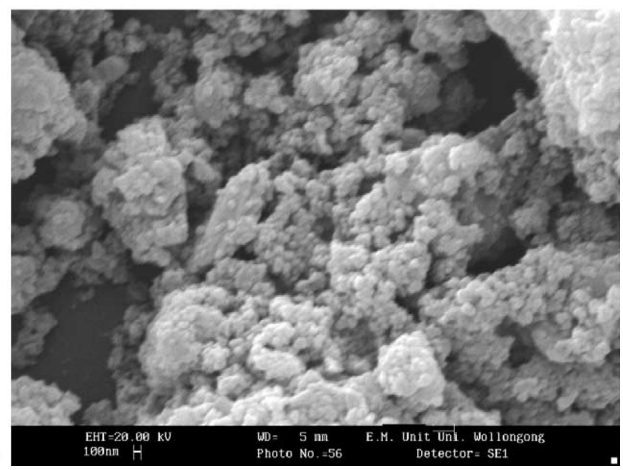

Fig. 2. (a) SEM image of ss-*o*-$LiMnO_2$ material; (b) typical SEM image of sg-*o*-$LiMnO_2$ material.

3.2. Electrochemical characteristics

Teflon test cells containing *o*-$LiMnO_2$ materials were cycled at room temperature. The cells were cycled in a voltage window of 2.0–4.4 V at a constant current density of 0.4 mA/cm^2. Fig. 3 shows the evolution of the discharge specific capacity versus the number of cycles. Following the phase transition occurring at the first charge, several cycles appear necessary for the materials to reach their optimal capacity, up to 18 cycles at a current density of 0.4 mA/cm^2 in the case of the ss-*o*-$LiMnO_2$ compounds, while the initial discharge capacity is just about 30 mAh/g. In contrast, the full capacity is obtained almost from the first cycle for the sg-*o*-$LiMnO_2$ material with $R = 0.5$. The initial capacity is more than 190 mAh/g at room temperature for the sg-*o*-$LiMnO_2$ ($R = 0.5$) sample. This is likely to be related to kinetic reasons, since in spite of very different reversible capacities, the discharge profiles of the ss-*o*-$LiMnO_2$ and sg-*o*-$LiMnO_2$ samples are the same (with two plateaux at ~4 and 3 V). This means that the ss-*o*-$LiMnO_2$ samples are likely to contain a substantial amount of unreacted *o*-$LiMnO_2$ phase, probably in the crystal core, i.e. covered by a spinel-type phase present at the crystal surface.

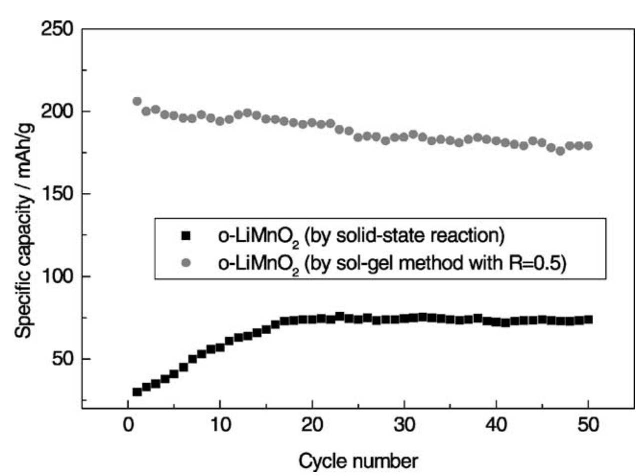

Fig. 3. Discharge specific capacity vs. cycle number of *o*-$LiMnO_2$ samples cycled at 0.4 mA/cm^2 in the 4.4–2.0 V range.

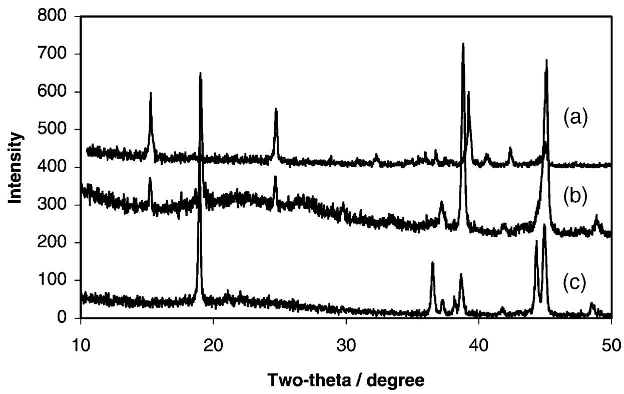

Fig. 4. (a) XRD pattern of o-$LiMnO_2$. Comparison between the X-ray diffraction patterns of (b) ss-o-$LiMnO_2$ compound and (c) sg-o-$LiMnO_2$ with $R = 0.5$ compound after 10 cycles at a current density of 0.4 mA/cm^2. Clearly the ss-o-$LiMnO_2$ material retains unreacted o-$LiMnO_2$.

In order to check this hypothesis, X-ray diffraction patterns were recorded for powders retrieved from the cell positive electrodes after several charge/discharge cycles (the ss-o-$LiMnO_2$ and the sg-o-$LiMnO_2$ with $R = 0.5$ phases are compared here) (Fig. 4). This study shows that after more than 10 cycles, o-$LiMnO_2$ is still present in the ss-o-$LiMnO_2$ materials, whereas it has completely disappeared in the sg-o-$LiMnO_2$ ($R = 0.5$) compound.

To investigate the kinetics of the electrode process, ac impedance measurements were conducted. The Nyquist plots obtained for ss-o-$LiMnO_2$ and sg-o-$LiMnO_2$ ($R = 0.5$) are shown in Fig. 5. EIS experiments were performed on working electrodes in the OCV state. Just one semicircle was observed in the OCV state for both samples. In the low frequency region a straight line was obtained which represents a diffusion-controlled process in the solid electrode. The semicircle might contain a contribution due to the compaction of particles in the composite cathode, i.e. the inter-particle contacts such as oxide–oxide, carbon–oxide and carbon–carbon contacts. Therefore, the reduction in the diameter of the arc in sg-o-$LiMnO_2$ ($R = 0.5$) probably can be ascribed to a decrease in the inter-particle contact resistance. Zview2.3C software was used to quantitatively analyze the condition of the cathode, and the situation at the o-$LiMnO_2$ electrode can be approximately represented by the equivalent circuit in Fig. 6. R_s is the solution resistance of the cell, R_{ct} is the cathode charge transfer resistance, C_{dl} represents the double layer capacitance, and W_o is a diffusion impedance, the $W_o - T$ value represents the Warburg coefficient, which is related to the diffusion coefficient of the lithium ions into the cathode by the formula: $W_o - T = L^2/D$ (L is the effective diffusion thickness, and D is the effective diffusion coefficient of the lithium ions). Table 2 lists the results calculated from ac impedance spectra based on the equivalent circuit shown in Fig. 6 using Zview2.3C software. It is obvious that the sg-o-$LiMnO_2$ ($R = 0.5$) compound has a lower charge-transfer resistance and a lower $W_o - T$, which may suggest that the lithium ions diffuse more easily into the sg-o-$LiMnO_2$ ($R = 0.5$) cathode than into the ss-o-$LiMnO_2$ cathode. All of this can be explained

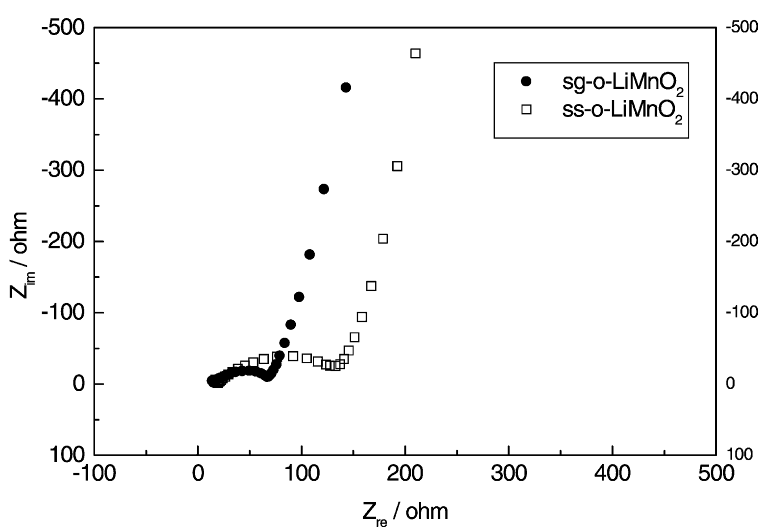

Fig. 5. EIS spectra (Nyquist complex plane plots) for cells with active electrodes of ss-o-$LiMnO_2$ and sg-o-$LiMnO_2$ with $R = 0.5$ at the OCV state.

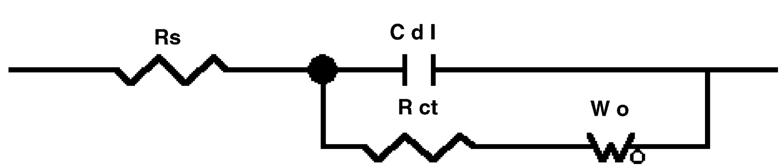

Fig. 6. Equivalent circuit for the o-$LiMnO_2$ electrode (R_s is the solution resistance of the cell, R_{ct} is the cathode charge transfer resistance, C_{dl} represents the double layer capacitance, and W_o is a diffusion impedance).

Table 2
Results of ac impedance analysis of the ss-o-$LiMnO_2$ and sg-o-$LiMnO_2$ ($R = 0.5$) compounds

Compounds	R_s	R_{ct}	C_{dl} ($\times 10^{-6}$)	$W_o - T$
ss-o-$LiMnO_2$	37.36	71.77	6.59	134.2
sg-o-$LiMnO_2$ ($R = 0.5$)	31.9	38.05	7.08	1.28

R_s is the solution resistance of the cell, R_{ct} is the cathode charge transfer resistance, C_{dl} represents the double layer capacitance, and W_o is a diffusion impedance, the $W_o - T$ value represents the Warburg coefficient.

by the smaller particle size and good homogeneity of sg-o-$LiMnO_2$. Smaller particle sizes can increase the Li^+-ion diffusion conductivity [16], and good homogeneity may improve the Li^+ diffusion in the cathode. Consequently, the improvement in the electrochemical performance of sg-o-$LiMnO_2$ ($R = 0.5$) may be explained by two factors, i.e. the reduction in the inter-particle contact resistance due to the smaller particle size and the increase of the diffusion efficiency of Li^+.

4. Conclusion

Orthorhombic $LiMnO_2$ was synthesized via the sol–gel process using citric acid as a chelating agent. XRD revealed that the samples with a high molar ratio of acid to metal ions R ($R = 1, 2$) contain an MnO impurity phase, while the sample with low R ($R = 0.5$) contains a monoclinic Li_2MnO_3 impurity phase. The presence of MnO could be detrimental to the electrochemical activity of the electrode, because MnO is electrochemically inactive. Therefore, the ratio of acid to metal ions should not be too high (lower than 1). sg-o-$LiMnO_2$ ($R = 0.5$) exhibited a high initial capacity, above 190 mAh/g when cycled at a current density of 0.4 mA/cm^2 at room temperature. The ac impedance results show that the initial capacity was improved (compared with the ss-o-$LiMnO_2$) due to the smaller particle size and good homogeneity which improved the Li^+ diffusion in the cathode.

References

[1] J.M. Tarascon, E. Wang, F.K. Shokoohi, J. Electrochem. Soc. 138 (1991) 2859.
[2] J. Barker, R. Koksbang, M.Y. Saidi, Solid State Ion. 82 (1995) 143.
[3] M.M. Thackeray, P.G. David, P.G. Bruce, J.B. Goodenough, Mater. Res. Bull. 18 (1983) 461.
[4] R.J. Gummow, D.C. Liles, M.M. Thackeray, Mater. Res. Bull. 28 (1993) 1249.
[5] A.R. Armstrong, P.G. Bruce, Nature 381 (1996) 499.
[6] L. Croguennec, P. Deniard, R. Brec, P. Biensan, M. Broussely, Solid State Ion. 89 (1996) 127.
[7] L. Croguennec, P. Deniard, R. Brec, J. Electrochem. Soc. 144 (1997) 3323.
[8] G.T.K. Fey, K.S. Chen, B.J. Huang, Y.L. Lin, J. Power Sources 68 (1997) 519.
[9] Y.M. Choi, S.I. Pyun, S.I. Moon, Y.E. Hyung, J. Power Sources 72 (1998) 83.
[10] Y.K. Sun, S.H. Jin, J. Mater. Chen. 8 (1998) 2399.
[11] X. Xi, G. Zaiping, N. Yanna, J. New Mater. Electrochem. Syst. 3 (2000) 327.
[12] Z.P. Guo, G.X. Wang, K. Konstantinov, H.K. Liu, S.X. Dou, J. Alloys Compounds 346 (2002) 255.
[13] W. Tang, H. Kanoh, K. Ooi, J. Solid State Cem. 142 (1999) 19.
[14] R.J. Gummow, M.M. Thackeray, J. Electrochem. Soc. 141 (1994) 1178.
[15] P. Barboux, J.M. Tarascon, F.K. Shokoohi, J. Solid State Chem. 94 (1991) 185.
[16] J. Kim, A. Manthiram, Electrochem. Solid State Lett. 2 (1999) 55.